Article

Morphology-Controlled DPA Nano Blocks as Electrochemiluminescence Emitters for MicroRNA Detection with One Step DNA Walker Amplification

Jia-Li Liu, Zhi-Ling Tang, Jia-Qi Zhang, Yaqin Chai, Ying Zhuo, and Ruo Yuan

Anal. Chem., **Just Accepted Manuscript** • DOI: 10.1021/acs.analchem.8b00209 • Publication Date (Web): 22 Mar 2018

Morphology-Controlled DPA Nano Blocks as Electrochemiluminescence Emitters for MicroRNA Detection with One Step DNA Walker Amplification

Jia-Li Liu, Zhi-Ling Tang, Jia-Qi Zhang, Ya-Qin Chai, Ying Zhuo*, Ruo Yuan*

Key Laboratory of Luminescent and Real-Time Analytical Chemistry (Southwest University), Ministry of Education, College of Chemistry and Chemical Engineering, Southwest University, Chongqing 400715,China.

* Corresponding authors at: Tel.: +86 23 68252277, fax: +86 23 68253172.

E-mail addresses: yingzhuo@swu.edu.cn (Y. Zhuo), yuanruo@swu.edu.cn (R. Yuan).

ABSTRACT

The electrochemiluminescence (ECL) properties of polycyclic aromatic hydrocarbons (PAHs) are excellent on account of the high photoluminescence quantum yield. However, the poor solubility and radical instability of PAHs in the aqueous solution severely restricted the further biological application. Here, 9,10 - diphenylanthracene (DPA) nano blocks (NBs) with good dispersibility and stability in aqueous solution were prepared according to morphology-controlled technology employing water-soluble polymers as a protectant. Furthermore, an ECL "off-on" switch biosensor was developed based on a novel ECL ternary system with DPA NBs as luminophore, dissolved O_2 as co-reactant, and Pt-Ag alloy nanoflowers as the co-reaction accelerator, which achieved a high-intense initial ECL signal. Subsequently, the Fc-DNA as ECL signal quencher were assembled on the electrode surface to quench the initial ECL signal for a "signal-off" state. Meanwhile, DNA swing arm was modified on the electrode surface for one step DNA walker amplification. Interestingly, in the presence of miRNA-141 and T7 Exo, the one step DNA walker amplification was executed to recover a strong ECL signal as a "signal on" state by the digestion of Fc-DNA. Thus, the developed ECL "off-on" switch biosensor possesses a detection limit down to 29.5 aM for ultrasensitive detection of miRNA-141, which is expected to be applicable to the detection of miRNA in clinic tumor cells.

KEYWORDS: 9,10 - diphenylanthracene, electrochemiluminescence, ternary system, one step target-cycling DNA walker amplification.

INTRODUCTION

MicroRNAs (miRNAs) are a kind of endogenetic, short, non-coding single stranded RNAs, which are significant regulators in biological processes.[1,2] Mounting evidences have indicated that abnormal (up- or down-regulation) expression of miRNAs are closely related to the pathogenesis of various types of human cancers. Significantly, miRNA-141 is a potentially reliable biomarker of prostate cancer.[3,4] However, the quantification of miRNAs suffers severe challenges in consequence of the low abundance of miRNAs.[5] Therefore, it is urgent to seek high specificity and sensitivity techniques for the detection of miRNAs. As a predominant technique in bioanalysis, electrochemiluminescence (ECL) combining the electrochemical and luminescent tools has received great attention with the advantages of high sensitivity, low luminescence background and simple operation.[6-8] Since the systematic study of ECL[9] was published in 1964, the development of ECL has experienced a history of more than 50 years.[10,11] During this time, the luminescence behaviour of polycyclic aromatic hydrocarbons (PAHs) and its derivates[12,13] has been widely investigated, owing to the high photoluminescence quantum yield and stable radical ions in aprotic solvent. Even though the ECL performance of PAHs was excellent, it still suffers the problem of the poor solubility in the aqueous solution and the radical instability because of the high reactivity between radical ions and water, which restricted the further application in food analysis, environmental monitoring, clinical diagnosis and other fields. Aimed at this situation, Bard's group prepared PAH nanoparticles (NPs) in aqueous phase by reprecipitation method, and observed the ECL emission behavior

with the TPrA or $NaClO_4$ as co-reactant.[14] Although the ECL of PAHs in aqueous solution was explored, the ECL intensity of those PAHs NPs was quite weak on account of the small diffusion coefficients of the NPs in the solution, and the PAHs NPs was unstable which grew into nanowires in a week due to the lack of surface protection. Recently, the morphology-controlled technology have attracted much attention.[15] In this case, amphiphile molecules containing hydrophilic groups and hydrophobic groups are employed to combine the material surface for controlling the morphology. Particularly, polyvinyl alcohol (PVA) as a water-soluble polymer, one's hydrophilic group oriented towards the water, while the hydrophobic carbon chains wrapped around the material surface, could increase the hydrophilicity and stability of nanomaterials by steric protection.[16] Thus, in this work, with the adsorption of PVA molecules on 9,10 - diphenylanthracene nano blocks (DPA NBs), the morphology-controlled electrochemiluminescence nanomaterials (Pt-Ag@DPA NBs) were synthesized to solve the problem of poor dispersibility and stability in aqueous solution.

Recently, DNA nanomachines propelled by strand-displacement[17,18] and enzymes[19,20] have drawn substantial research effort, for instance, DNA walkers,[21] DNA nanogears,[22] DNA tweezers[23] and so on. Particularly, with the imitation of biological protein motors to move directionally along the track, the DNA walkers have been applied in biological fields as signal amplification strategies. Li's group utilized microRNA (miRNA) as a driving force to design a novel DNA walker biosensor which combined the strand displacement cascades with enzymatic recycling

cleavage strategy. In addition, our previous work constructed a novel bi-directional DNA walker machine which achieved the dual miRNA detection through the migration of the DNA walker along the track to change the ECL signal.[24] However, the traditional DNA walkers were impelled by a strand displacement reaction with the sequential addition of fuel strands to achieve the movement,[25,26] which was complex, time-consuming and accompanying the duplex waste. Recently, autonomous DNA walkers based on the enzymatic cleavage of DNA have gradually attracted the attention of researchers which avoided repeatly adding multiple DNA to maintain the motion of DNA walkers.[27] Furthermore, with the help of enzymes, a 3D DNA walker with all DNA components on the same AuNP to increase their local effective concentrations has been established to accelerate the enzymatic cleavage for payload release or biosensing.[28] However, this strategy was usually executed with separate operation by two steps which exhibited complex operation with the disposable use of target. To simplify the operation and realize the target cycle, we designed a one step DNA walker on electrode surface to rapidly and efficiently achieve signal amplification.

Herein, we combined the one step DNA walker amplification on the electrode interface and an original ECL ternary system to develop an ECL “off-on” biosensor for ultrasensitive detection of miRNA-141 from cancer cells. Initially, as shown in Scheme 1A, the Pt-Ag@DPA NBs, a combination of DPA NBs as luminophore and Pt-Ag alloy on the DPA NBs as co-reaction accelerator, were synthesized and modified on the electrode surface for an extremely strong ECL signal in the presence

of dissolved O_2 as co-reactant. Besides, the Pt-Ag alloy on the DPA NBs could further assemble the Fc-DNA (the DNA strand labelled with ferrocene) as ECL signal quencher to quench ECL signal for a "signal-off" state. Meanwhile, DNA swing arm was modified on the electrode surface for one step DNA walker amplification. Interestingly, as depicted in Scheme 1B, the DNA swing arm on the electrode was made up of DNA1 and DNA2 by complementary base pairing to restrict the hybridization between DNA2 and Fc-DNA on the electrode. However, when the reaction solution containing miRNA-141 and T7 Exo were incubated on the electrode, the miRNA-141 captured the DNA1 to form a double-stranded structure which released the DNA2 to combine the Fc-DNA on the electrode surface. As expected, with the help of T7 Exo, which could digest the blunt or recessed 5′ termini of DNA in RNA/DNA hybrids or double-stranded DNA (dsDNA)[29,30] to shear the DNA into pieces, the miRNA-141 was released for the combination with other DNA1 to achieve the target recycle. Meanwhile, Fc-DNA could also be released from electrode surface, and the DNA2 as walking strand were free to hybridize with another Fc-DNA again to initiate the DNA walker recycling processes. Significantly, based on the one step DNA walker amplification on the electrode interface, an enormous ECL signal was recovered as a "signal on" state. As a result, the ECL response increased gradually with the increasing miRNA-141 concentrations from 100 aM to 1 nM. Thus, the proposed method combining the novel ECL ternary system and one-step DNA walker amplification strategy blazed a new trail for highly sensitive detection of miRNA-141, which is hopeful to be applied in clinical tumor cells.

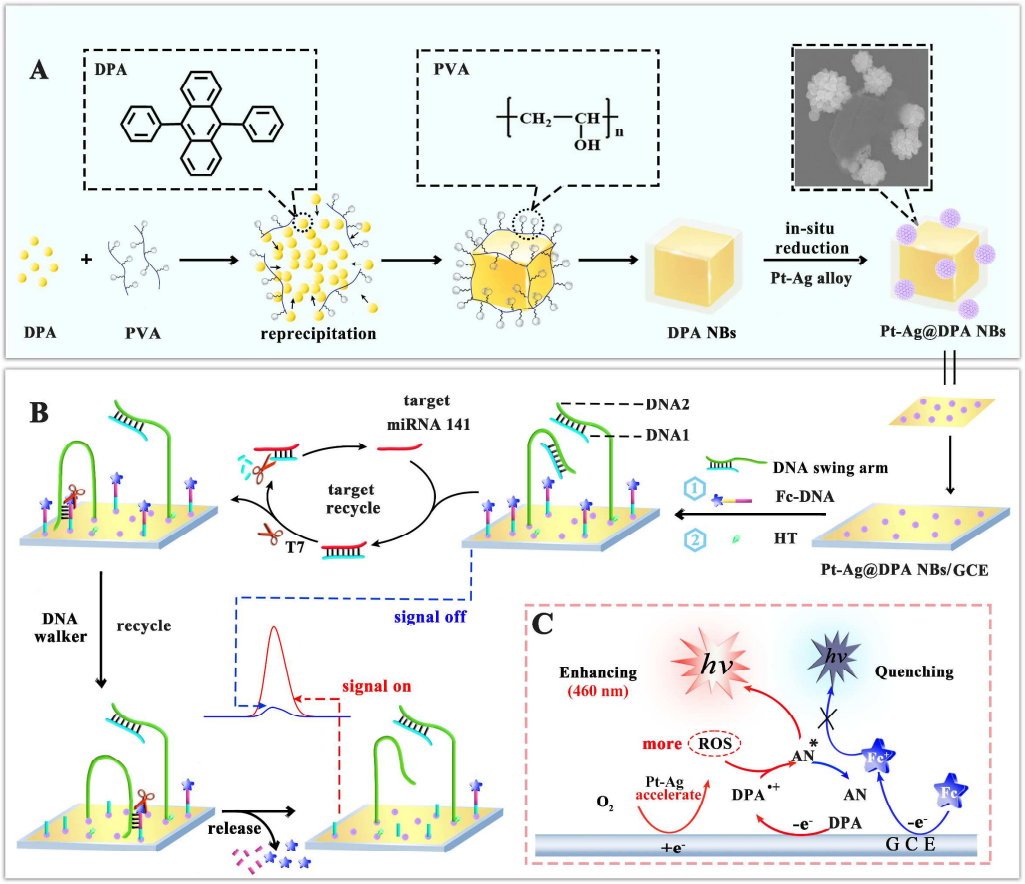

Scheme 1. The schematic illustration of the preparation of Pt-Ag@DPA NBs (A), ultrasensitive detection of miRNA-141 based on the one step DNA walker amplification (B), and the possible ECL mechanism of Pt-Ag@DPA NBs (C).

EXPERIMENTAL SECTION

Preparation of DPA NBs. The reprecipitation method with minimal modification was used to synthesize the DPA nano blocks (NBs).[31] First, 3 mg DPA powder was dissolved in 3 mL acetone to prepare a homogeneous DPA solution (1 mg/mL). Next, the PVA aqueous solution was obtained by mixing PVA powder (50 mg) with 10 mL deionized water at 60 °C under stirring. Then, the DPA solution was quickly injected into the above PVA aqueous solution with vigorous stirring for 10 min, followed by

stewing over night in dark place. Then, the DPA NBs were obtained after centrifugation and washing with deionized water for several times.

Formation of Pt-Ag@DPA NBs. 24 μL of 1% H_2PtCl_6 was mixed with 10 mL of the DPA NBs solution. Then, 50 μL of 0.1 M AA was added in the above solution with vigorous stirring for 5 h at 30 °C water bath. After the color of the solution changing from ivory to gray, we speculated that the PtNPs was wrapped on the DPA NBs. Subsequently, 40 μL of 10 mM $AgNO_3$ and 20 μL of H_2PtCl_6 (1%) were dissolved in 10 mL of the DPA NBs solution with stirring. After that, 40 μL of AA (0.1 M) was added to reduce the Pt-Ag alloy on the precoated DPA NBs. With agitating at 30 ℃ water bath for 5 h, the color of the solution transformed to dark grey for the generation of Pt-Ag@DPA NBs.

Preparation of the Basal Solution. The basal solution were prepared according to the reported work with some modifications.[32] First, 100 μL solution of the mixture solution containing 5 μM DNA1 oligonucleotides and 2.5 μM DNA2 oligonucleotides were heated to 95 °C for 5 min and slowly cooled down to room temperature to obtain a composite structure named as DNA swing arm. Afterward, 10 μL of them and 10 μL of 25 μM Fc-DNA were blended in the 80 μL Tris-HCl buffer to acquire the basal solution.

Fabrication of Biosensor. First, the glassy carbon electrode (GCE) was pretreated using our previous method.[33] The as-prepared bare GCE was then modified with 8 μL Pt-Ag@DPA NBs solution. After being dried in air, the modified electrode was

incubated with 10 μL basal solution for 12 h at 4 °C. Then, the decorated electrode was rinsed with 1 × TE buffer and blocked with 1.0 mM HT for 40 min.

One Step DNA Walker Amplification. Briefly, the reaction solution were composed of 1 × NE buffer 4, target miRNA-141 (with various concentrations) and 100 U/mL T7 Exo. Subsequently, the reaction solution was dropped on the as-prepared biosensor to incubate at 25 °C for 3 h (the feasibility analysis of the target-cycling amplification was supplied in Supporting Information). After rinsing with 1 × TE buffer to remove the unbound residue, the ECL and electrochemical measurements were operated.

ECL Measurement Procedure. The obtained biosensor was detected in 2 mL PBS (pH 7.4) to investigate the ECL response with a MPI-A ECL analyzer. Besides, the ECL potential scanning ranged from -1 to 1.2 V with the voltage of the photomultiplier tube (PMT) at 800 V.

RESULTS AND DISCUSSION

Morphology and Structure Characterization of Different Nonmaterials. The morphologies of as-synthesized DPA NBs and Pt-Ag@DPA NBs were characterized by scanning electron microscopy (SEM). Figure 1A showed the feature of DPA NBs with a uniform size. The DPA NBs exhibited a block-like structures with side length of 400 ± 100 nm. When the Pt-Ag alloy were reduced to the surface of DPA NBs, the image was observed clearly with a great difference compared to the individual DPA NBs. As illustrated in Figure 1B, the dispersity of nanomaterials was improved, and the Pt-Ag alloy with a hydrangea-like structure grew on the DPA NBs surface. The

DPA NBs with block-like structures became more transparent than the single DPA NBs due to the superior conductivity of Pt-Ag alloy which increased the contrast between the DPA NBs and Pt-Ag alloy. Furthermore, XPS spectra of the Pt-Ag@DPA NBs were depicted in Figure 1C. Typically, the characteristic peaks of 284.5 eV, 533.3 eV for C1s, O1s could be observed clearly. Besides, as shown in Figure 1D, two characteristic peaks of 73 eV and 76 eV were obtained, which were attributed to 4f7/2 4f5/2 of Pt. Also, the binding energy at 368 eV and 374 eV (Figure 1E) exhibited the 3d5/2 and 3d3/2 features of Ag, which were attributed to the presence of Ag nanomaterials. Based on the elemental analysis, we could demonstrate that the Pt and Ag form an alloyed on the DPA NBs.

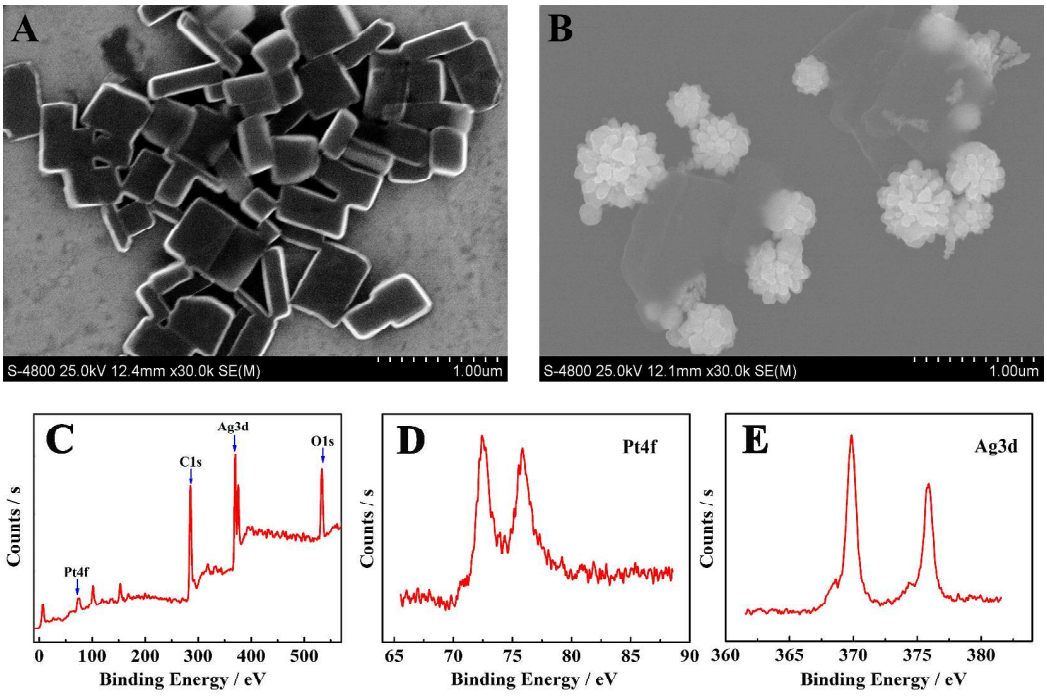

Figure 1. SEM images of (A) the DPA NBs and (B) the Pt-Ag@DPA NBs. XPS spectra of (C) the full region of Pt-Ag@DPA NBs, (D) the Pt4f region, and (E) Ag3d region.

UV−Vis Absorption, Fluorescence and ECL spectra of the DPA NBs. Furthermore,

the optical properties of DPA NBs were explored by UV-vis spectrometer and fluorescence (FL) spectrophotometer. The UV-vis absorption spectra of DPA dissolved in acetone and DPA NBs in an aqueous solution were displayed in Figure 2A, respectively. As shown in curve a, the UV-vis absorption spectra of DPA in acetone exhibited a broad band at 320-400 nm with three characteristic absorption peaks of 338, 354, 372 nm, while the UV-vis absorption spectra of DPA NBs (curve b) were red shifted by 10 nm. Similarly, compared to the FL spectra of DPA in acetone (curve c), the FL emission spectra of DPA NBs (curve d) in water showed bathochromic shift from 426 nm to 441 nm. Those red shift in the absorption and emission spectra of DPA NBs had been ascribed to the polarizable environment of the surrounding NBs in aqueous solution, which lowers the energy of the transition.[34] Additionally, as shown in the inset of Figure 2B, the as-prepared DPA NBs solution was pale grey under ambient daylight, but intuitively exhibited vibrant blue color with the radiation of UV lamp (λ = 365 nm). Meanwhile, Figure 2B depicted the ECL emission spectra (curve b) of DPA NBs with the maximum wavelength at 470 nm, which was slightly red-shift (441 to 470 nm) compared with the FL spectra (curve a) because of the self-absorption of DPA NBs[35] and instrument effects.[36]

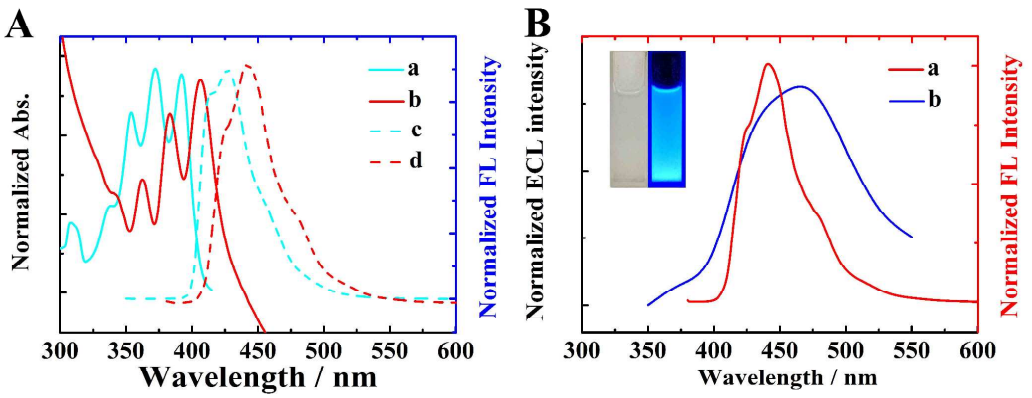

Figure 2. (A) UV-vis absorption spectra of (a) DPA dissolved in acetone, (b) DPA NBs in an aqueous solution, The FL spectra of (c) DPA dissolved in acetone, (d) DPA NBs in an aqueous solution. (B) The FL spectra of (a) DPA NBs in an aqueous solution with the 368 nm excitation wavelengths, (b) the ECL emission spectra of DPA NBs. The inset of B: images of DPA NBs under the ambient daylight (left) and the 365 nm UV light (right).

ECL Enhancement Mechanism of the Pt-Ag@DPA NBs and the Quenching Mechanism by Ferrocene. In order to investigate the ECL enhancement mechanism of DPA NBs with Pt-Ag alloy on the surface of DPA NBs, the ECL and its corresponding CV curves of DPA NBs and Pt-Ag@DPA NBs modified electrode were recorded. Under the potential scan of -1.0 to 1.2 V, the ECL and CV curves of the DPA NBs were displayed in Figure 3A. Obviously, a weak ECL signal about 395 a.u. was obtained, accompanying a small reduction peak at about -0.63 V with low currents which attributed to the reduction of dissolved O_2 in solution.[37] However, when the Pt-Ag@DPA NBs were decorated on the electrode, the ECL signal was raised to 16106 a.u. (Figure 3B) which was probably 41 folds higher than that of the individual DPA NBs. The possible enhancement mechanism was that the Pt-Ag alloy in situ growth on the DPA NBs could act as the co-reaction accelerator of dissolved

O_2 to generate more ROS (such as $O_2^{\bullet-}$, $OH^{\bullet}$)[38] constituting a novel ternary ECL system with DPA NBs as luminophore.

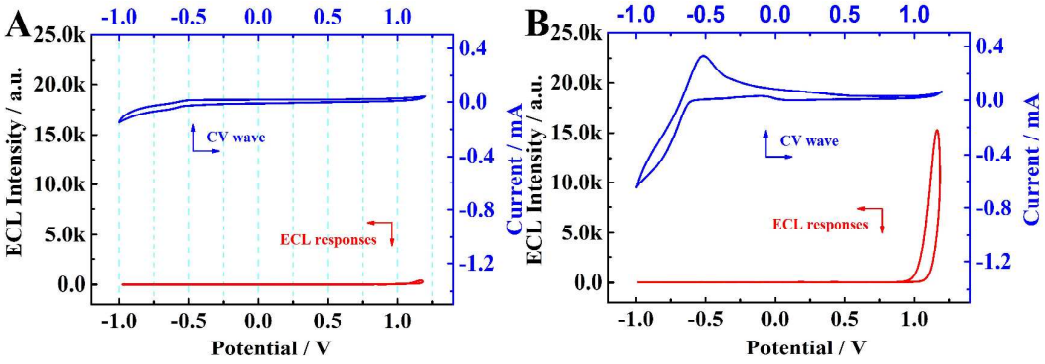

Figure 3. ECL-potential profiles (red line) and its corresponding CV curves (blue line) of (A) the DPA NBs, (B) Pt-Ag@DPA NBs.

Specifically, the agminated O_2 on the surface of the Pt-Ag@DPA NBs was reduced to produce massive $O_2^{\bullet-}$ and $OH^{\bullet}$ (eq 1-3) with the help of the Pt-Ag alloy as co-reaction accelerator. Then, the DPA lost an electron to generate DPA radical cations ($DPA^{\bullet+}$) under the positive potential (eq 4). Finally, the $DPA^{\bullet+}$ interacted with $O_2^{\bullet-}$and $OH^{\bullet}$ respectively (eq 5,6) for the generation of the anthracene (AN) excited state species (AN*), which further made for an intense ECL emission from AN* to AN (eq 7). Consequently, the possible ECL enhancement mechanism was depicted as the following equations, and the schematic diagram of the possible ECL mechanism of ECL ternary system was depicted in Scheme 1C.

$$O_2 + e^- \xrightarrow{\text{Pt-Ag}} O_2^{\bullet -} \quad [1]$$

$$O_2 + 2H_2O + 2e^- \xrightarrow{\text{Pt-Ag}} H_2O_2 + 2OH^- \quad [2]$$

$$O_2^{\bullet -} + H_2O_2 \longrightarrow O_2 + OH^- + OH^{\bullet} \quad [3]$$

$$DPA - e^- \longrightarrow DPA^{\bullet +} \quad [4]$$

$$DPA^{\bullet +} + O_2^{\bullet -} \longrightarrow AN^* + O_2 + \text{product} \quad [5]$$

$$DPA^{\bullet +} + OH^{\bullet} \longrightarrow AN^* + OH^- + \text{product} \quad [6]$$

$$AN^* \longrightarrow AN + h\nu \quad [7]$$

As shown in Scheme 1B, when the Fc-DNA were assembled on the electrode surface decorated with Pt-Ag@DPA NBs, a weak ECL response was observed as the "singnal off" state (blue line) because of the quenching effect of ferrocene.[39] First, the Fc(II) reacted with O_2 to form Fc(III) (eq 8), which consumed the dissolved O_2 as the co-reactant of the ECL system to result in the decrease of ECL intensity. Then, the Fc(III) could be reduced to Fc(II) (eq 9) under cathodic scanning to regenerate the Fc(II) for scavenging O_2. On the other hand, the ferrocene also availably quenched the ECL signal of DPA due to electron transfer mechanisms. Finally, after the reaction of one step DNA walker amplification, the “signal on” state (red line) with strong ECL intensity was obtained because the ferrocene fell off the electrode. The possible ECL quenching mechanism was depicted as the following equations:

$$4Fc(II) + O_2 + 2H_2O \longrightarrow 4Fc(III) + 4OH^- \quad [8]$$

$$Fc(III) + e^- \longrightarrow Fc(II) \quad [9]$$

Optimal Conditions for the ECL Biosensor. In order to achieve the optimal experimental performance, the concentration ratio of DNA swing arm/Fc-DNA in the basal solution and the incubation times of the biosensor with both the basal solution

and the reaction solution were investigated. Since the DNA swing arm and Fc-DNA were supported on electrode surface simultaneously, the concentration ratio of DNA swing arm/Fc-DNA were optimized to obtain the best performance for subsequent magnification strategy. When adjusted the concentration ratio from 1:1 to 1:12, the ECL response results were shown in Figure 4A. As we can see, the ECL intensity decreased dramatically, due to the quenching of ferrocene. Finally, we chosen a ratio of 1:10 to prepare the basal solution. With the increase of the incubation time, a growing number of Fc-DNA and DNA swing arm were captured on the surface of the electrode, which enhanced the quenching efficiency to reduce the ECL intensity (Figure 4B). When the incubation time was up to 12 h, the ECL intensity tended to be stable, indicating the saturated capture of Fc-DNA and DNA swing arm. As a result, 12 h was used as the optimal incubation time of the basal solution. Furthermore, after dropping the reaction solution on the proposed electrode, the reaction time of the one step DNA walker amplification was also been explored. As displayed in Figure 4C, the ECL signal enhanced gradually as the reaction time increased, and a stable ECL intensity could be achieved at 3 h, which was chosen as the optimal reaction time.

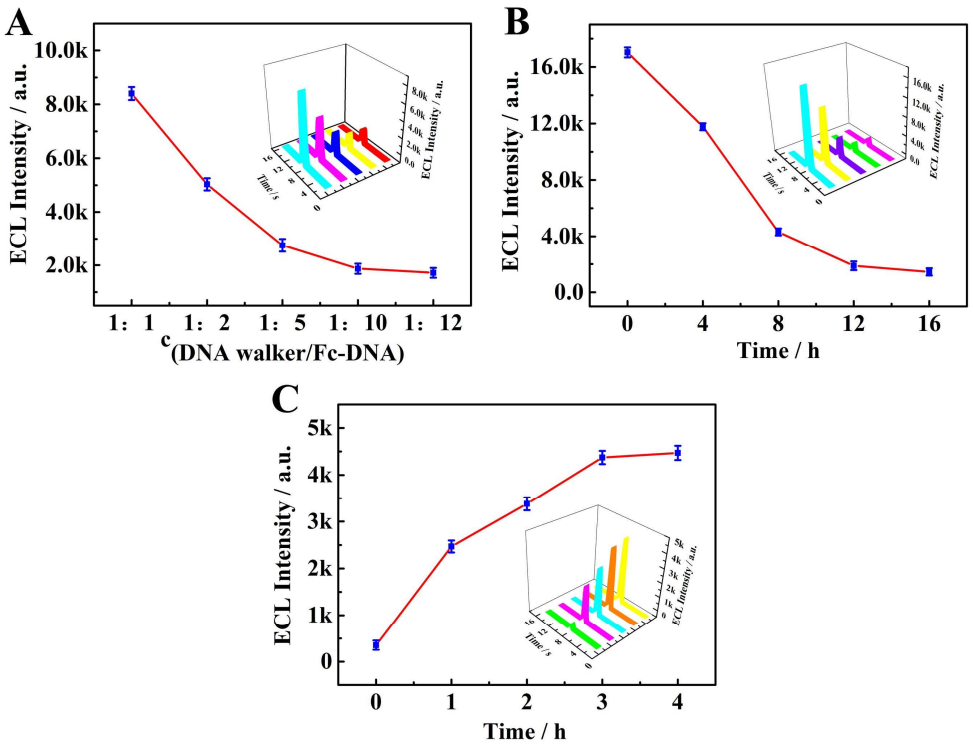

Figure 4. The optimization of (A) the concentration ratio of DNA swing arm/Fc-DNA, (B) the incubation time of the basal solution on the electrode, (C) the reaction time of the one step DNA walker amplification at 1 fM miRNA-141.

Characterization of the ECL Biosensor. To characterize the stepwise fabrication process of the biosensor, the ECL and EIS analysis technique were utilized, respectively. As can be seen in Figure 5A, the bare electrode had almost no ECL response (curve a). After the Pt-Ag@DPA NBs were modified on the electrode surface, a remarkable ECL signal of 16100 a.u. was achieved in curve b, due to the presence of luminophore and co-reaction accelerator. When the basal solution was incubated on the modified GCE, the ECL intensity declined promptly (curve c), attributing to the quenching effect of the Fc-DNA and the obstruction of DNA swing which were captured on the electrode surface, simultaneously. Subsequently, the ECL

signal further decreased because the HT could obstruct the electron transfer (curve d). However, the ECL intensity (curve e) recovered partially after the reaction solution containing 1 fM miRNA-141 were incubated on the modified GCE, for the DNA walker removed the Fc-DNA on the electrode surface with the help of T7 Exo.

Besides, Figure 5B exhibited the EIS plots of the fabrication process at each step. The bare GCE showed a small semicircle (curve a), due to the low electron-transfer resistance (R_{et}) value of the $Fe(CN)_6^{3-/4-}$. The R_{et} of the Pt-Ag@DPA NBs (curve b) was increased slightly after the Pt-Ag@DPA NBs was decorated on the electrode, which is attributed that the thin film on the electrode surface hindered the electron transfer. When the modified electrode was incubated with the basal solution and HT, successively, the R_{et} kept increasing (curve c,d) owing to the fact that the negatively charged DNA repelled $[Fe(CN)_6]^{3-/4-}$ from the surface of the electrode. As expected, with the operation of one step DNA walker amplification on the electrode surface, the Fc-DNA on the electrode were digested by the T7 Exo to acquire a decreased R_{et} (curve e). The above results of the EIS were consistent with the ECL characterization, suggesting the successful construction of the proposed ECL biosensor.

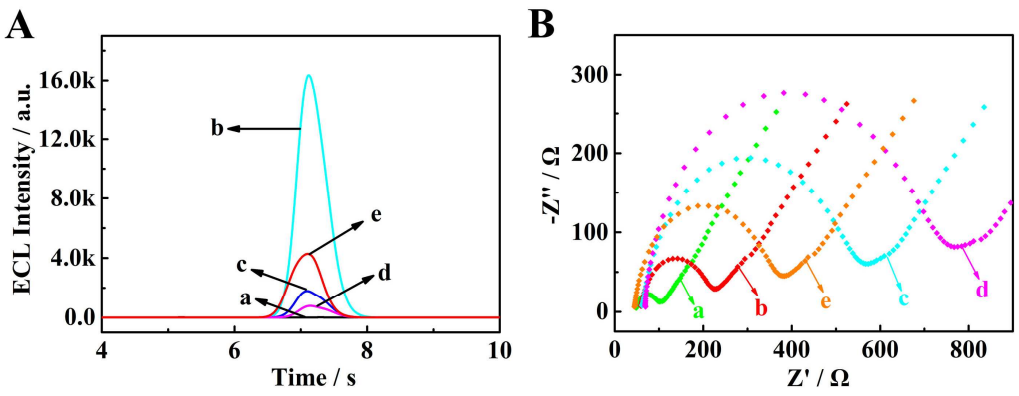

Figure 5. Characterization of biosensors with stepwise fabrications based on ECL (A) and EIS (B). (a) bare GCE, (b) Pt-Ag@DPA NBs/GCE, (c) DNA swing arm/Fc-DNA/Pt-Ag@DPA NBs/GCE, (d) HT/DNA swing arm/Fc-DNA/Pt-Ag@DPA NBs/GCE, (e) after reaction/HT/DNA swing arm/Fc-DNA/Pt-Ag@DPA NBs/GCE.

ECL Measurement of the Proposed Biosensor. Under the optimal conditions, the quantitative measurements of the proposed ECL biosensor were implemented with the "off-on" mode. As depicted in Figure 6A, the ECL intensity increased with the increasing miRNA-141 concentration from 100 aM to 1 nM. The ΔI_{ECL} exhibited a good positive correlation with the logarithmic value of miRNA-141 concentration, and the regression equation of ΔI = 31093.13 + 1827.5 lg$c$ was obtained with a correlation coefficient of 0.9975 (Figure 6B). The detection limit was evaluated to be 29.5 aM at a signal-to-noise ratio (S/N) of 3. As a result, we could determine that the proposed biosensor exhibited high sensitivity with a much lower detection limit. Besides, the comparison results between the proposed assay and other reported methods were listed in Table 1.

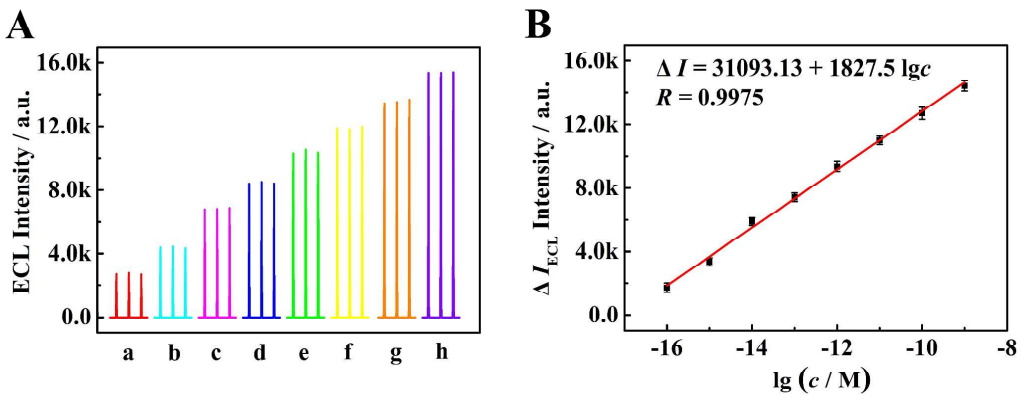

Figure 6. (A) The standard ECL responses of the as-proposed biosensor for the detection of

miRNA-141 with different concentration: 100 aM, 1 fM, 10 fM, 100 fM, 1 pM, 10 pM, 100 pM, 1 nM (from a to h). (B) The calibration curve for the relationship between the ΔI_{ECL} intensity and the logarithm of miRNA-141 concentration.

Table 1. Comparison of Different Methods for MiRNA Detection.

detection method	signal amplification strategy	linear range	analysis time	detection limit	ref
Fluorescence	AuNP-based hairpin-locked DNAzyme	200 pM~150 nM	480 min	25 pM	40
Fluorescence	enzyme-free DNA nanowheels	2 fM~2 nM	160 min	0.8 fM	41
SERS	enzyme-free DNA machine	1 fM~100 nM	120 min	0.17 fM	42
ECL	3D DNA Walking Machine	10 fM~100 pM	300 min	3.3 fM	43
ECL	Target-Cycling DNA Walker	100 aM~1 nM	180 min	29.5 aM	This work

Selectivity and Stability of the ECL Biosensor. To measure the ECL performance of the as-prepared biosensor, selectivity and stability were two kinds of essential elements. Hence, different miRNAs including miRNA-155, miRNA-21, and miRNA-199a were employed as interfering substances to investigate the selectivity of the biosensor. As shown in Figure 7A, compared to the blank solution (absence of target miRNA-141), the ECL intensity of the proposed biosensor significantly increased in the presence of miRNA-141 (1 nM). However, when the miRNA-155

(100 nM), miRNA-21 (100 nM), and miR-199a (100 nM) were used to replace the target miRNA-141, respectively, the ECL signal of those interfering substances exhibited no obvious increase compared with the blank. After mixing the miRNA-155 (100 nM), miRNA-21 (100 nM), and miRNA-199a (100 nM) with the target miRNA-141 (1 nM), the ECL response showed an enormous ECL intensity which was no remarkable difference with that of 1 nM miRNA-141 only. The consequences illustrated that the proposed biosensor exhibited outstanding selectivity. Furthermore, the stability of the as-prepared biosensor was depicted in Figure 7B. Under continuous cyclic potential scan for 32 cycles, the ECL intensity of the biosensor didn't exhibit apparent undulation (RSD = 1.21%) in the presence of 1 fM miRNA-141, which implied that the stability of the proposed biosensor was excellent.

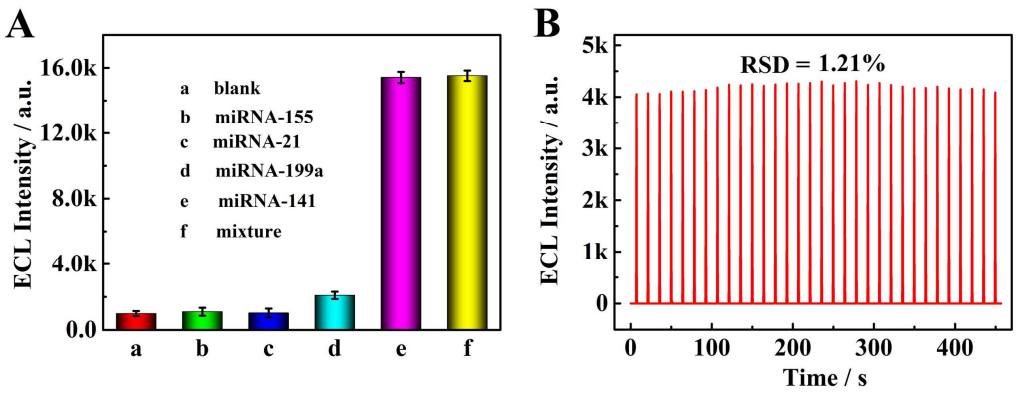

Figure 7. (A) Selectivity of the ECL biosensor with different targets. Error bars, SD, n = 3. (B) Stability of the proposed biosensor under continuous cyclic potential scan for 32 cycles.

Preliminary Analysis of the Biosensor in Tumor Cells. To evaluate the feasibility of the developed biosensor in real samples, the lysates from 22Rv1 (human prostate carcinoma cells) with high expression of miRNA-141 and MCF-7 (human breast

cancer cells) with low expression of miRNA-141 were employed to execute an ECL assay to measure the expression of miRNA-141 in tumor cells. After cell counting, the sensitivities of the proposed biosensor were investigated by increasing the cell concentrations from 10 cells to 10^6 cells. As depicted in Figure 8, when the MCF-7 concentrations increased from 10 cells to 10^6 cells, the ECL response increased tardily, indicating the low expression of miRNA-141 in the MCF-7 cells. However, the ECL response was enhanced significantly in the presence of the extraction from 22Rv1 cells with the concentration variation from 10 cells to 10^6 cells, which implied the high expression of miRNA-141 in the 22Rv1 cells.

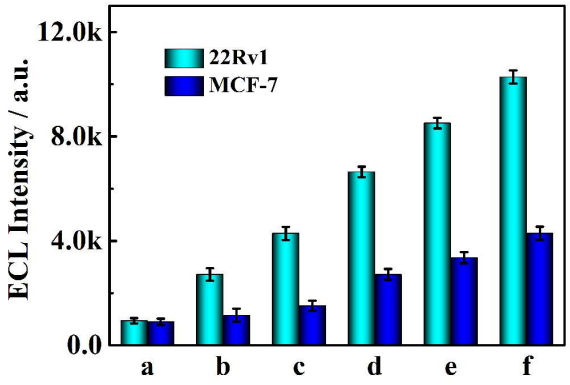

Figure 8. The detection of miRNA-141 in 22Rv1 and MCF-7 with the proposed biosensor. (a) 10 cells, (b) 10^2 cells, (c) 10^3 cells, (d) 10^4 cells, (e) 10^5cells, and (f) 10^6 cells.

Conclusion

In conclusion, highly efficient ECL of Pt-Ag@DPA NBs was observed based on the novel ECL ternary switch platform with DPA NBs as luminophore, Pt-Ag alloy as co-reaction accelerator and the dissolve O_2 as co-reactant in the aqueous solution. Significantly, with the one step DNA walker amplification on the electrode interface,

the as-prepared biosensor could achieve the target recycle and enzymatic cleavage simultaneously, which exhibited simple manipulation and high sensitivity for the detection of miRNA-141. Thus, combined with a novel ECL ternary system and one step DNA walker amplification on the electrode interface, the developed ECL "off-on" switch biosensor possesses a detection limit as low as 29.5 aM which exerted great application potential in bioanalysis and early clinical diagnoses of cancer.

ASSOCIATED CONTENT

Supporting Information

Reagents and apparatus, gel electrophoresis for the feasibility analysis of the target-cycling amplification, possible ECL mechanism of Pt-Ag@DPA NBs, and the response reproducibility of the biosensor were supplied in Supporting Information.

AUTHOR INFORMATION

*** Corresponding authors**

Tel.: +86 23 68252277, fax: +86 23 68253172.

E-mail addresses: yingzhuo@swu.edu.cn (Y. Zhuo), yuanruo@swu.edu.cn (R. Yuan).

Notes

The authors declare no competing financial interest.

Acknowledgements

This work was financially supported by the NNSF of China (21675129, 51473136, 21575116, 21775124), and the Fundamental Research Funds for the Central Universities (XDJK2015A002), China.

REFERENCES

(1) Calin, G. A.; Croce, C. M. *Nat. Rev. Cancer*, **2006**, 6, 857-866.

(2) Bartel, D. P. *Cell*, **2004**, 116, 281-297.

(3) Jou, A. F., Lu, C. H., Ou, Y. C., Wang, S. S., Hsu, S. L., Willner, I., Ho, J. A. A. *Chem. Sci.*, **2015**, 6, 659-665.

(4) Nie, Y. M., Zhang, P., Wang, H. J., Zhuo, Y., Chai, Y., Yuan, R. *Anal. Chem.*, **2017**, 89, 12821-12827.

(5) Cheng, G. Adv. *Drug Deli. Rev.*, **2015**, 81, 75-93.

(6) Tan, X.; Zhang, B.; Zou, G. Z. *J. Am. Chem. Soc.* **2017**, 139, 8772-8776.

(7) Liu, Z.; Qi, W.; Xu, G. *Chem. Soc. Rev.* **2015**, 44, 3117-3142.

(8) Bard, A. J. Electrogenerated Chemiluminescence; Marcel Dekker: New York, **2004**.

(9) Hercules, D. M. *Science* **1964**, 145, 808-809.

(10) Marcus, R. A. *J. Chem. Phys.* **1965**, 43, 2654-2657.

(11) Abruña, H. D.; Bard, A. J. *J. Am. Chem. Soc*. **1982**, 104, 2641-3642.

(12) Chandross, E. A.; Sonntag, F. I. *J. Am. Chem. Soc*. **1964**, 86, 3179-3180.

(13) Faulkner, L. R.; Bard, A. J. *J. Am. Chem. Soc*. **1968**, 90, 6284-6290.

(14) Omer, K. M.; Bard, A. J. *J. Phys. Chem. C.* **2009**, 113, 11575-11578.

(15) Kang, L. T.; Wang, Z. C.; Cao, Z. W.; Ma, Y.; Fu, H. B.; Yao, J. N. *J. Am. Chem. Soc.* **2007**, 129, 7305-7312.

(16) Sato, T.; Ruch, R. Stabilization of Colloidal Dispersions by Polymer Adsorption; Surfactant Science Series, No.9; Marcel Dekker: New York, **1980**.

(17) Shin, J. S.; Pierce, N. A. *J. Am. Chem. Soc.* **2004**, 126, 10834-10835.

(18) Jung, C.; Allen, P. B.; Ellington, A. D. *Nat. Nanotechnol*. **2016**, 11, 157-163.

(19) Bath, J.; Green, S. J.; Turberfield, A. J. *Angew Chem. Int. Ed.* **2005**, 117, 4432-4435.

(20) Wickham, S. F. J.; Bath, J.; Katsuda, Y.; Endo, M.; Hidaka, K.; Sugiyama, H.; Turberfield, A. J. *Nat Nanotechnol*. **2012**, 7, 169-173.

(21) Pan, J.; Li, F.; Cha, T. G.; Chen, H.; Choi, J. H. *Curr. Opin. Chem. Biol.* **2015**, 34, 56-64.

(22) Zhang, P.; Lin, Z.; Zhuo, Y.; Yuan, R.; Chai, Y. Q. *Anal. Chem.* **2017**, 89, 1338-1345.

(23) Elbaz, J.; Moshe, M.; Willner, I. *Angew. Chem. Int. Ed.* **2009**, 121, 3892-3895.

(24) Peng, L.; Zhang, P.; Chai, Y. Q.; Yuan, R. *Anal. Chem.* **2017**, 89, 5036-5042.

(25) Sherman, W. B.; Seeman, N. C. *Nano Letters* **2004**, 4, 1203-1207.

(26) Shin, J. S.; Pierce, N. A. *J. Am. Chem. Soc.* **2004**, 126, 10834-10835.

(27) Delius, M.; Leigh, D. A. *Chem. Soc. Rev.* **2011**, 40, 3656-3676.

(28) Yang, X.; Tang, Y.; Mason, S. D.; Chen, J.; Li, F. *ACS nano* **2016**, 10, 2324-2330.

(29) Liu, X.; Li, W.; Hou T, Dong, S.; Li, F. *Anal. Chem.* **2015**, 87, 4030-4036.

(30) Zhang, H.; Li, M.; Li, C.; Guo, Z.; Dong, H.; Wu, P.; Cai, C. *Biosens. Bioelectron.* **2015**, 74, 98-103.

(31) Park, D. H.; Jo, S. G.; Hong, Y. K.; Cui, C.; Lee, H.; Ahn, D. J.; Joo, J. *J. Mater. Chem.* **2011**, 21, 8002-8007.

(32) Zhao, M.; Chen, A. Y.; Huang, D.; Chai, Y. Q.; Zhuo, Y.; Yuan, R. *Anal. Chem.* **2017**, 89, 8335-8342.

(33) Zhang, P.; Lin, Z.; Zhuo, Y.; Yuan, R.; Chai, Y. Q. *Anal. Chem.* **2017**, 89, 1338-1345.

(34) Kim, H. Y.; Bjoklund, T. G.; Lim. S.H.; Bardeen, C. J. *Langmuir* **2003**, 19, 3941.

(35) Rashidnadimi, S.; Hung, T. H.; Wong, K. T.; Bard, A. J. *J. Am. Chem. Soc.* **2008**, 130,

634-639.

(36) Nepomnyashchii, A. B.; Pistner, A. J.; Bard, A. J.; Rosenthal, J. *J. Phys. Chem. C.* **2013**, 117, 5599-5609.

(37) Hayyan, M.; Hashim, M. A.; AlNashef, I. M. *Chem. Rev.* **2016**, 116, 3029-3085.

(38) Zhou, Y.; Wang, H.; Zhuo, Y.; Chai, Y. Q.; Yuan. R. *Anal. Chem.* **2017**, 89, 3732-3738.

(39) Cao, W.; Ferrance, J. P.; Demas, J.; Landers, J. P. *J. Am. Chem. Soc.* **2006**, 128, 7572-7578.

(40) Yang, Y.; Huang, J.; Yang, X.; He, X.; Quan, K.; Xie, N.; Wang, K. *Anal. Chem.* **2017**, 89, 5850-5856.

(41) Gong, X.; Zhou, W.; Chai, Y. Q; Yuan, R.; Xiang, Y. *Chem. Commun.* **2016**, 52, 2501-2504.

(42) Li, X.; Ye, S.; Luo, X. *Chem. Commun.* **2016**, 52, 10269-10272.

(43) Xu, Z. Q.; Liao, L. L.; Chai, Y. Q.; Wang, H. J.; Yuan, R. *Anal. Chem.* **2017**, 89, 8282-8287.

For TOC only

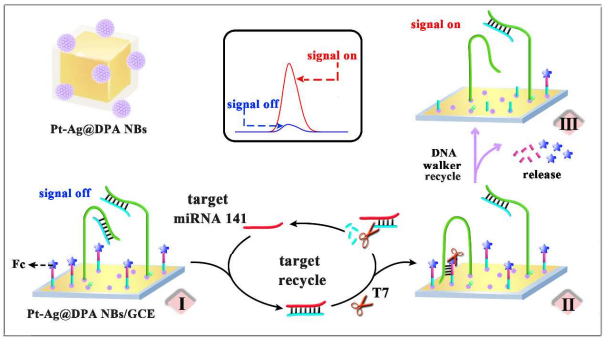
Pt-Ag@DPA NBs
signal on
signal off
signal on
III
DNA
walker
recycle
release
signal off
target
miRNA 141
Fc
target
recycle
T7
Pt-Ag@DPA NBs/GCE
I
II